Journal of
Low Power Electronics and Applications

MDPI

Communication

Design of Impedance Matching Network for Low-Power, Ultra-Wideband Applications

Sepideh Hassani, Chih-Hung Chen * and Natalia K. Nikolova

Department of Electrical and Computer Engineering, McMaster University, Hamilton, ON L8S 4L8, Canada; hassas52@mcmaster.ca (S.H.); talia@mcmaster.ca (N.K.N.)
* Correspondence: chench@mcmaster.ca; Tel.: +1-(905)-525-9140 (ext. 27084)

Abstract: This paper addresses the design of ultra-wideband (UWB) impedance matching networks operating in the unlicensed 3.1–10.6 GHz frequency band for low-power applications. It improves the simplified real frequency technique (SRFT) by adding a realizability check and employing an iterative approach with different initial guesses in optimization to achieve realizable solutions under the requirements of UWB, low-power consumption, and a minimum number of circuit components. The comparison of solutions obtained using the SRFT with published solutions based on the Chebyshev filter theory is presented. It is shown that the optimal SRFT solution requires fewer components in the impedance matching network, maximizes the RF power delivery over the UWB spectrum with a reflection coefficient below −10 dB, and allows for circuit optimization to reduce power consumption. Using the improved SRFT, it demonstrates a systematic approach to find the strategies and limitations of designing the input matching networks for low-power UWB applications using GlobalFoundries 90 nm BiCMOS technology.

Keywords: ultra-wideband (UWB); impedance matching network; simplified real frequency technique

check for updates

Citation: Hassani, S.; Chen, C.-H.; Nikolova, N.K. Design of Impedance Matching Network for Low-Power, Ultra-Wideband Applications. *J. Low Power Electron. Appl.* **2024**, *14*, 16. https://doi.org/10.3390/jlpea14010016

Academic Editor: Amlan Ganguly

Received: 29 January 2024
Revised: 14 March 2024
Accepted: 16 March 2024
Published: 19 March 2024

1. Introduction

Ultra-wideband (UWB) technology is characterized by exceptional features, such as high data rate, low power spectral density, enhanced target recognition, precise localization, and ranging capabilities [1]. These qualities make UWB a desirable choice for a wide variety of applications, including wireless communication, radar, and imaging. In these applications, the primary focus is ensuring the optimal transmission and reception of signals within the operational bandwidth. Hence, the design of broadband impedance matching networks (IMN) has emerged as a significant area of interest for engineers [2].

To match a source impedance Z_S to an arbitrary load impedance Z_L, as illustrated in Figure 1, various theories and techniques have been developed. To meet this objective, Fano [3] and Youla [4] invoked the gain-bandwidth limitation theory and utilized the Darlington representation, where the load Z_L is represented by a lossless two-port terminated in a unit resistor. Analytical models for determining the IMN are also used, but they require an analytical model of the load impedance [5] and often result in suboptimal solutions in terms of circuit performance metrics and network complexity [6].

Another approach to the design of passive IMNs relies on filter theory [7–10]. The approach employs either a cascaded L-section topology consisting of high-pass and low-pass filters [7,8] or a bandpass filter [9,10]. These fixed topologies, however, may not necessarily provide a minimum number of elements in the IMN for a specific load [6]. A related approach employs series or tank resonators, and it is based on manipulations of the resonant frequencies [11,12]. When these resonant frequencies can be strategically spaced apart while maintaining an acceptable gain variation, it is possible to attain a broadband IMN. However, it may not prove effective for high fractional bandwidth (FBW) requirements, where many resonators are required.

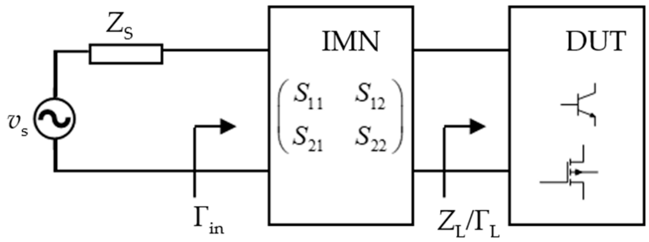

Figure 1. Matching an arbitrary load impedance Z_L to a source impedance Z_S.

Design approaches for IMNs with no prior assumption about the network topology, no need for analytical load modelling, and leading to a minimum element count have always been desired. To fulfill this need, Carlin [5] developed the so-called real frequency technique (RFT) utilizing the real-frequency (e.g., experimental) load-impedance data along with numerical optimization. The initial version of the RFT technique was to solve a single matching problem, i.e., a complex load impedance Z_L with a source impedance Z_s = 50 Ω [5]. The subsequently developed RFTs can be classified into four distinct categories, namely the line segment technique (RFT-LST), the direct computational technique (DCT), the parametric approach, and the simplified real frequency technique (SRFT) [2]. The line segment technique, direct computational technique, and parametric approach formulate the objective function utilizing the unknown input immittance (driving point admittance or impedance) across the entire angular real-frequency ω axis. The procedure starts with the real part of the input immittance, as the imaginary part would be found with the Hilbert transformation or the Gewertz procedure. A lossless two-port IMN can be synthesized by finding an optimized input immittance. The line segment technique formulates the real part of the input immittance as a linear combination of straight lines $R_{\text{in}} = \sum_{k=1}^{N} a_k(\omega)R_k$ [5]. On the other hand, the direct computational technique defines the real part of a positive real minimum immittance as a rational even function $R_{\text{in}}(\omega) = Ev\{Z_{\text{in}}(s)\}|_{s=j\omega} = \frac{N(\omega^2)}{D(\omega^2)}$ [13]. The parametric approach represents this rational function in a parametric form $Z_{\text{in}}(s) = \sum\limits_{k=1}^{N} \frac{A_k}{s+s_k}$ and takes the even function of Z_{in} as the real part of Z_{in} [14]. Finally, the simplified real frequency technique simplifies the task by defining the two-port scattering parameters of an IMN as rational functions [15], which helps in handling the double-matching problems [13,16] and streamlining the computation process [17].

In this paper, we present the simplified real frequency technique in detail in Section 2 and apply this technique to the design of the IMN for low-power applications in Section 3, followed by the conclusions.

2. Simplified Real Frequency Technique (SRFT)

The SRFT starts with defining the scattering parameters, S_{IMN}, of an IMN containing lossless reciprocal passive elements based on three polynomials: h, g, and f. Because the IMN should satisfy the paraunitary requirement $S^{\dagger}_{\text{IMN}} \cdot S_{\text{IMN}} = \boldsymbol{I}$ [17–19], where $\boldsymbol{I}$ is the identity matrix, S_{IMN} is expressed as

$$S_{\text{IMN}} = \begin{bmatrix} S_{11} = \frac{h(s)}{g(s)} & S_{12} = \frac{f(s)}{g(s)} \\ S_{21} = \frac{f(s)}{g(s)} & S_{22} = \frac{-(-1)^k \cdot h(-s)}{g(s)} \end{bmatrix} \tag{1}$$

where $h(s)$ and $g(s)$ are polynomials of order n, n is the number of elements in an IMN, and $k = 0, 1, 2, \ldots, n$. The polynomial $g(s)$ is strictly Hurwitz, which has all poles on the left-hand side of the complex plane to avoid impractical or unrealizable solutions. The polynomial $f(s)$ provides the information about the transmission zeros of the IMN. Transmission zeroes are defined as the frequencies at which the output signal is completely cut off. In consideration of a transmittance function S_{21} that may possess finite zeros at $\pm j\omega_i$, zeros at infinity, or zeros at the origin, its general form is expressed as

$$f(s) = s^k \prod_{i=1}^{m} (s^2 + \omega_i{}^2) \tag{2}$$

Such form implies that $f(s)$ can be either an odd function or an even function. The presence of finite zeros, such as in the modified Chebyshev design [20], often increases the number of elements and complicated synthesis [21]. Therefore, it is preferable for $f(s)$ to be in the s^k form. The parameter k may assume a value of zero in low-pass scenarios and a value greater than one in bandpass and high-pass cases [22]. The lossless condition introduces a relationship among the polynomials f, g, and h. Knowing $f(s)$ allows for expressing $g(s)$ as a function of $h(s)$ as

$$g(s)g(-s) = h(s)h(-s) + f(s)(-s) \tag{3}$$

The objective in designing the IMN for a known load can be achieved by either maximizing the transductor power gain G_{T}, ideally approaching unity, or minimizing the reflection coefficient Γ_{in}, as follows from

$$G_{\mathrm{T}} = \frac{|S_{21}|(1 - |\Gamma_{\mathrm{L}}|^2)}{|1 - S_{22}\Gamma_{\mathrm{L}}|^2} \tag{4}$$

and

$$\Gamma_{\mathrm{in}} = S_{11} + \frac{S_{21}S_{12}\Gamma_{\mathrm{L}}}{1 - S_{22}\Gamma_{\mathrm{L}}} \tag{5}$$

The SRFT utilizes optimization techniques to determine the optimal polynomial $h(s)$ and, consequently, the corresponding polynomial $g(s)$. Optimization aims to minimize the error function based on the objective function (4) or (5) for load impedance data.

3. Results and Discussion

3.1. Comparing SRFT and Chebyshev Filter-Based Solutions

Bode and Fano demonstrated a physical limitation on the maximum achievable bandwidth for loads comprising resistors and reactive elements [3,23]. For example, in the case of a load with a resistor R and capacitor C connected in series, this limitation can be found by [24]

$$\int_0^{\infty} \frac{1}{\omega^2} \ln\left[\frac{1}{|\Gamma_{\mathrm{in}}(\omega)|}\right] d\omega < \pi RC \tag{6}$$

It is evident from (6) that efficient broadband impedance-matching structures inherently exhibit filter-like characteristics [23,24]. For optimal matching performance, all reflection coefficients $|\Gamma_{\mathrm{in}}(\omega)|$ within the frequency band of interest are preferred to be small while $|\Gamma_{\mathrm{in}}(\omega)|$ outside this frequency range are one (i.e., perfect reflection). So, the sharper the cut-off rate of the filter is, the better the performance of the IMN will be [25]. It is well known that the Chebyshev filter offers a sharper cut-off; therefore, it is chosen for comparison with the SRFT method. In [9], a UWB Chebyshev filter theory was used to design the IMN for a load modelled by a 50 Ω resistor in series with a 650 fF capacitor. The IMN comprises five components, with their values (from [9]) depicted in Figure 2. The reflection coefficient resulting from this design is shown in Figure 3, obtained by simulating the circuit in Figure 2 using the Cadence Virtuoso Spectre circuit simulator with ideal elements from the analog library.

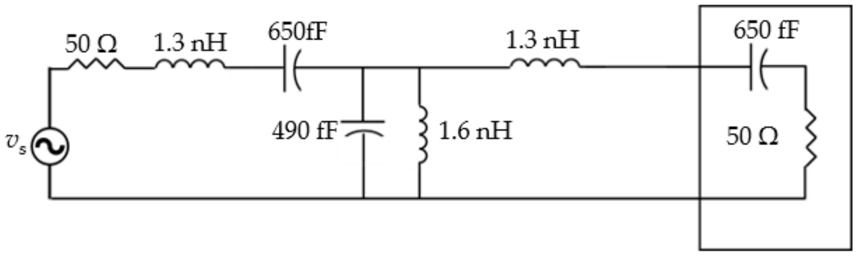

Figure 2. UWB IMN based on the Chebyshev filter theory in [9].

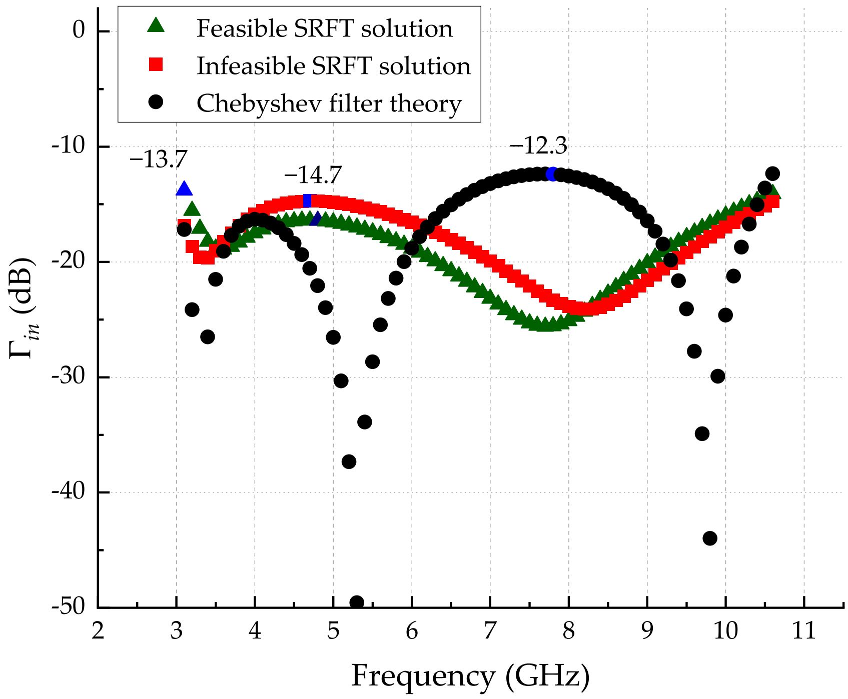

Figure 3. Reflection coefficient of the design using the Chebyshev filter theory (●) [9], the SRFT-based realizable solution (▲), and the SRFT-based unrealizable solution (■). The maximum Γ_{in} of each response is indicated by the blue color symbols.

On the other hand, when designing a UWB IMN using SRFT, the choice of the optimization method plays a significant role in obtaining a solution with better performance. Most reported RFT and SRFT techniques use Levenberg–Marquart optimization [15,17,26], a local optimization algorithm that aims to find the minimum of a function in the vicinity of an initial guess. Thus, it is best suited for problems where a solution is expected to be found in the proximity of the initial guess [27]. Selecting a good initial guess in such a highly nonlinear optimization process is critical, and it substantially impacts the ability to reach the optimal IMN [15,22,28].

To see if we can obtain a better solution than the Chebyshev filter approach, we applied the SRFT to the same load as in [9]. It is observed that the SRFT may yield solutions that cannot be realized by LC elements, even if they demonstrate superior matching performance. We characterize them as unrealizable solutions. One such solution is shown by the red symbols in Figure 3. The realizability of a solution can be verified by examining the input reflection coefficients observed at the input port of the IMN when its output port is terminated with either a short or an open circuit. For example, when the IMN comprises solely reactive elements, and when the output port is open-circuited, its input reflection coefficient $\Gamma_{\text{in,OC}}$ or input impedance $Z_{\text{in,OC}}$ can be expressed in terms of $f(s)$, $h(s)$, and $g(s)$ as

$$\Gamma_{\text{in,OC}}(s) = S_{11}(s) + \frac{S_{12}^2(s)}{1 - S_{22}(s)} = \frac{h(s)\left[g(s) + (-1)^k h(-s)\right] + f^2(s)}{g(s)\left[g(s) + (-1)^k h(-s)\right]} = \frac{N(s)}{D(s)} \quad (7)$$

and

$$\begin{aligned} Z_{\text{in,OC}}(s) &= \tfrac{1+\Gamma_{\text{in,OC}}(s)}{1-\Gamma_{\text{in,OC}}(s)} = \tfrac{D(s)+N(s)}{D(s)-N(s)} \\ &= k_n s^n + k_{n-1}s^{n-1} \ldots + k_1 s + k_0 + \tfrac{k_{p0}}{s} + \tfrac{k_{p1}}{s-j\omega_{p1}} + \tfrac{k'_{p1}}{s+j\omega_{p1}} \ldots \end{aligned} \quad (8)$$

where $N(s)$ and $D(s)$ are the numerator and denominator of the input reflection coefficient. In (8), the input impedance $Z_{\text{in,OC}}$ is expressed in a partial-fraction form, where k_i is the coefficient of s^i, k_{pi} and k'_{pi} are residues, and ω_{pi} are poles. Since the input impedance $Z_{\text{in,OC}}$ only comprises reactive components, it should exhibit the following three characteristics. First, it must be an odd function (k_0 = 0) with the numerator and denominator differing by one degree. Second, it should contain only simple zeros and poles, all interlaced on the $j\omega$ axis. Third, the residues of $Z_{\text{in,OC}}$ for all poles must be real-positive [29]. If a solution violates any of these features, it cannot be implemented only by reactive elements. For instance, the red curve in Figure 3 is not realizable because of its $k_0 < 0$.

To find a realizable solution, an exhaustive search with various initial guesses using the Levenberg–Marquardt optimization method is required. In the SRFT, it assigns initial-guess values to the $n + 1$ coefficients of $h(s)$. Each coefficient value is randomly selected from a continuous uniform distribution within the bounds defined by l_b and u_b for quick optimization convergence [30]. If the solution fails to satisfy the feasibility conditions outlined above, another initial guess is used until a realizable solution is found. Based on this iterative approach, a solution with a maximum reflection coefficient of −13.7 dB in the whole UWB spectrum has been found, as shown by the green symbols in Figure 3. This solution is better than the solution obtained using the Chebyshev filter theory, which features a maximum reflection coefficient of −12.3 dB [9]. Moreover, the solution obtained using the SRFT requires only four elements, as demonstrated in Figure 4, as opposed to the five elements required by the Chebyshev design. This is beneficial, particularly in this example, saving space since an inductor is eliminated.

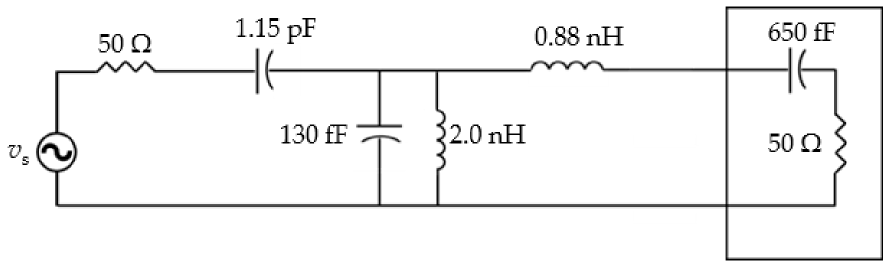

Figure 4. UWB IMN based on the SRFT.

Another way to verify the performance of an IMN solution for a particular load is to check how close it is to the Bode–Fano limit, πRC in (6). As $|\Gamma_{\text{in}}(\omega)|$ in (6) cannot be determined using an analytical expression in SRFT, it is assumed that $|\Gamma_{\text{in}}(\omega)|$ remains constant and equal to an average value Γ_{avg} across the specified frequency band. This approximation can simplify (6) as [24]

$$\frac{BW}{\omega_0^2} \ln\left(\frac{1}{\Gamma_{\text{avg}}}\right) < \pi RC \quad (9)$$

where $BW = \omega_{\max} - \omega_{\min}$, $\omega_0 = \sqrt{\omega_{\max}\omega_{\min}}$, and $\omega_{\min}$ and $\omega_{\max}$ are the lower and upper limits of the frequency band. For the realizable solution shown in Figure 3, the averaged reflection coefficient Γ_{avg} is 0.115. This results in 78 ps, closer to the Bode–Fano limit of 102 ps compared with the 72 ps value obtained from [9].

As an alternative, one may consider utilizing global optimization techniques. These methods can offer the lowest possible reflection coefficient at the expense of significantly longer computations. RFT-based techniques predominantly employ local minimum optimization methods, yielding a solution quickly. As exemplified above, SRFT may result in an unrealizable solution, in which case another search must be initiated. With a global optimization method, e.g., the genetic algorithm (GA), the algorithm may bypass a realizable solution and converge to an unrealizable solution due to its inclination towards achieving the lowest minimax objective. Indeed, [31] reports an approach using the GA; however, impractical responses are sometimes obtained. It is clear that synthesizing a realizable solution for a UWB IMN (topology and component values) is problematic. While the optimization may indicate the existence of a solution, it may be difficult or even impossible to synthesize a practical network, particularly in scenarios involving intricate configurations and components like transformers. As shown in [32], some preassumption is required to find the right synthesis.

3.2. IMN for Low-Power Applications

Assuming the antenna provides a source impedance Z_S = 50 Ω in the frequency band of interest, the improved SRFT can find an IMN to match a load Z_L to the 50 Ω source impedance, as shown in Figure 1. The inductor-degenerated topology is a commonly used technique [33] for amplifiers using bipolar junction transistors (BJT) [34] and field-effect transistors (FET) [35]. Figure 5 shows the frequently used common emitter amplifier with a degeneration inductor L_e to obtain the required input resistance for narrowband [34] and wideband matching [10]. Here, C_1 serves as a DC blocking capacitor, and L_1 is an RF choke to isolate the biasing circuit from the RF port. We demonstrate the designs of the input matching networks based on the improved SRFT for different bias conditions and circuit topologies using GlobalFoundries 90 nm BiCMOS technology.

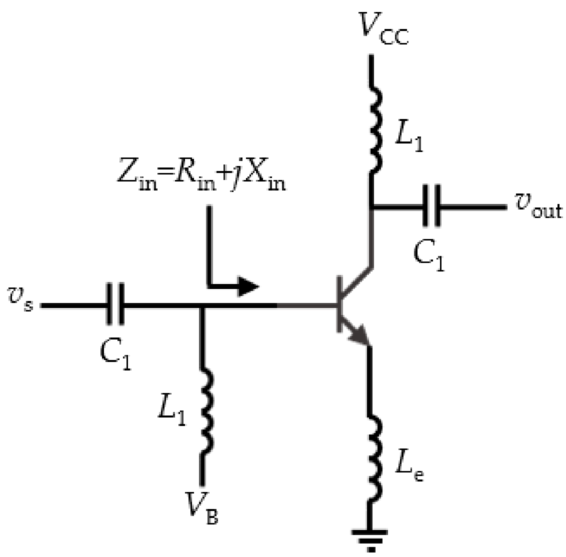

Figure 5. Inductively degenerated common-emitter amplifier.

For low-power applications, the circuit's input reactance sets the lower power consumption limit. When we reduce the power consumption by decreasing the base-to-emitter voltage applied to the BJT, the base-emitter junction capacitor (C_{be}) becomes smaller, resulting in a smaller C_{in} (or a bigger absolute value of input reactance) and a lower Bode–Fano limit, which makes it more challenging to find an IMN solution with $\Gamma_{in} < -10$ dB. To examine the lowest power consumption for the inductive degeneration topology shown in Figure 5 and ensure the circuit has sufficiently high cut-off frequency f_T to cover the

3.1–10.6 GHz band, Figure 6 shows the equivalent C_{in} at 3 GHz, the f_T of the transistor, and the f_T of the amplifier (with L_e in the range of 30–40 pH) at different collector currents I_C. The transistor used in the simulation has a length and width of 90 nm and 10 µm, respectively, and its collector is biased at 1.0 V. To be able to compare with the result in [9] and ensure that we can obtain a realizable IMN solution with $\Gamma_{in} < -10$ dB over 3.1–10.6 GHz, we start with the collector current I_C = 32.8 mA, at which C_{in} is about 650 fF, which is the same as the value reported in [9]. As expected, the reduction in the collector current decreases the equivalent input capacitance C_{in} at 3 GHz due to the reduction in C_{be}. The lowest collector current for a realizable IMN solution is at I_C = 27.4 mA. Further reducing C_{in} is prohibited by the Bode–Fano limit in (9). The R_{in} of this circuit exhibits frequency-dependent variations due to the inherent characteristics of the BJT transistor in this technology. The intrinsic base resistance varies from approximately 50 Ω to 17 Ω across the frequency band of interest. The adjustment of this variation around 50 Ω with the assistance of L_e poses an additional challenge in the quest for an IMN compared to a circuit that provides a constant 50 Ω over the bandwidth. In addition, comparing the circuit's cut-off frequency (f_T) and the transistor's f_T at these bias points indicates that the emitter degeneration inductor L_e enhances the f_T of the circuit slightly and follows the f_T of the transistor.

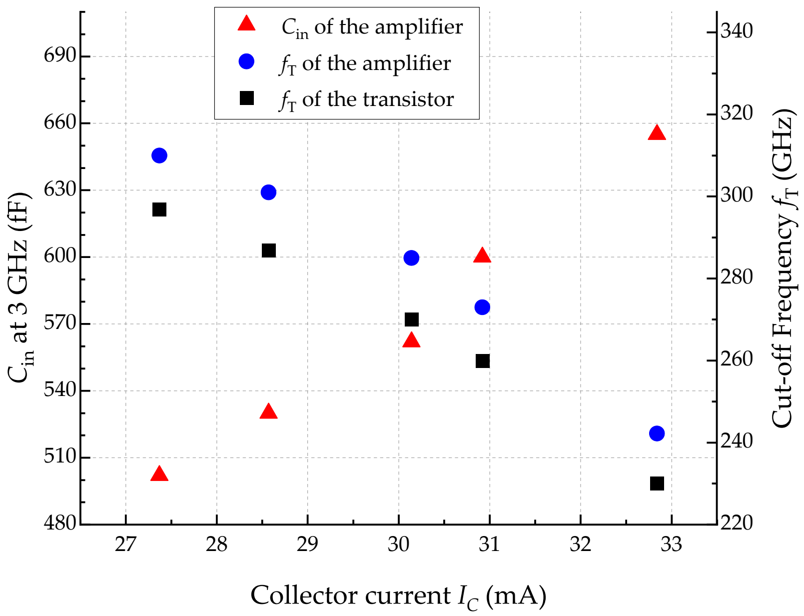

Figure 6. The equivalent input capacitance C_{in} (▲) at 3 GHz and the f_T (●) of the inductive degeneration common-emitter amplifier in Figure 5 with L_e in the range of 30–40 pH and the f_T (■) of the transistor at different collector currents I_C. The transistor used in the simulation has a length and width of 90 nm and 10 µm, respectively, and its collector is biased at V_{CC} = 1.0 V.

To further reduce the power consumption, C_{in} is to be established by adding a capacitor C_p in parallel at the amplifier input, as shown in Figure 7. Incorporating C_p mitigates variations in R_{in} with respect to frequency as it is placed in parallel with the intrinsic impedance of the transistor. This arrangement brings R_{in} closer to 50 Ω. When reducing the collector current I_C, we adhere to two essential criteria: (1) ensuring that the IMN remains below −10 dB across the bandwidth and (2) maintaining the circuit's f_T above 100 GHz to ensure a circuit bandwidth up to 10.6 GHz. C_p and L_e are adjusted to ensure that Z_{in} and f_T meet these requirements. Figure 8 shows the equivalent C_{in} at 3 GHz, the cut-off frequencies f_T of the transistor and the amplifier (with L_e in the range of 60–140 pH) at different collector currents I_C. It is observed that, although adding C_p decreases the f_T of the amplifier, we can further reduce the collector current I_C to 6.1 mA. When comparing with the initial I_C = 32.8 mA, we observe an 81.3% reduction in collector current while maintaining the f_T at around 100 GHz to ensure the amplifier operates at 10.6 GHz. A further decrease in the collector current I_C would yield a circuit with a reduced f_T or Γ_{in} surpassing −10 dB. Table 1 shows the component values of the IMN, C_p, and L_e for the bias conditions of the base-to-emitter voltage V_{BE} and the collector current I_C in Figure 8.

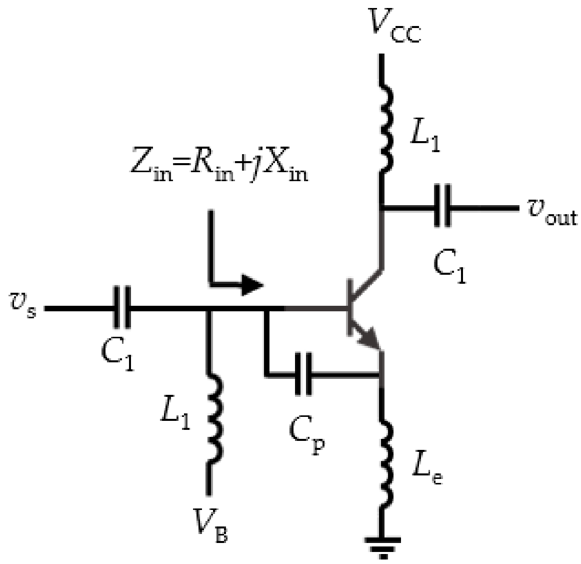

Figure 7. An inductively degenerated common-emitter amplifier with a capacitor C_p connected in parallel to the input of the amplifier.

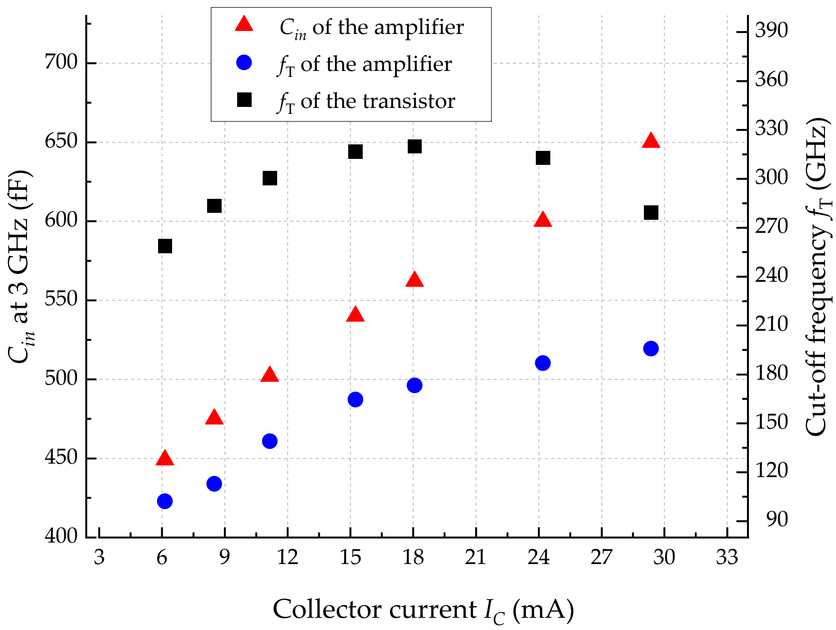

Figure 8. The equivalent input capacitance C_{in} (▲) at 3 GHz and the f_T (•) of the inductive degeneration common-emitter amplifier with C_P and L_e in Figure 7 and the f_T (■) of the transistor at different collector currents I_C. The transistor used in the simulation has a length and width of 90 nm and 10 µm, respectively, and its collector is biased at V_{CC} = 1.0 V.

Table 1. Component values for the amplifier in Figure 9 with V_{CC} = 1.0 V.

Parameter \ C_{in} (fF)	655	600	562	540	502	475	449
V_B (mV)	923	910	894	886	873	863	852
I_C (mA)	29.3	24.2	18.0	15.2	11.1	8.5	6.1
L_e (pH)	60	60	75	80	90	110	140
C_p (fF)	100	140	180	195	210	220	230
C_{11} (pF)	1.01	0.92	0.92	0.87	0.93	0.79	0.79
L_{12} (nH)	2.09	2.2	2.23	2.17	2.18	2.25	2.56
C_{12} (fF)	180	111	158	134	140	116	61
L_{22} (nH)	1.02	0.91	1.15	1.11	1.17	1.25	1.21
I_{Cmin} (mA)	25	21.46	15.9	13.42	10.85	8.5	6.1
I_{Cmax} (mA)	34.5	30.5	24.2	22.7	17.7	10.8	11.4

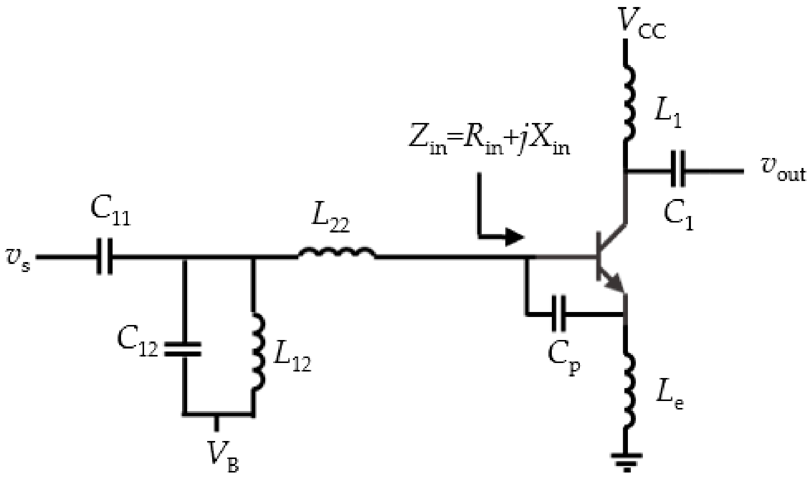

Figure 9. Inductively degenerated common-emitter amplifier with its UWB IMN.

Based on the amplifier shown in Figure 7, Figure 9 shows the complete amplifier design with its input IMN. Table 1 shows the component values of the circuit for the bias conditions in Figure 8. The I_{Cmax} and I_{Cmin} specify the tolerable range of the collector current to which the IMN solution can still maintain $\Gamma_{in} < -10$ dB over 3.1–10.6 GHz. Maintaining the tolerance for I_{Cmin} at low bias currents is challenging because C_{in} and the resulting Bode–Fano limit reduce, and, therefore, it is hard to find a solution with $\Gamma_{in} < -10$ dB.

4. Conclusions

We demonstrated that the SRFT is a highly efficient design method for UWB IMNs, which provides solutions with the minimum component count in the IMN. On the other hand, we also show that not all optimal reflection-coefficient responses obtained with the SRFT can be assured to be realizable or synthesizable. The choice of the optimization method and the initial guess are essential for uncovering solutions in RFT-based methodologies. With local optimization, which is usually employed by the SRFT methods, an improper initial point can result in a solution that is optimal in a mathematical sense but is physically unrealizable with components such as capacitors and inductors. On the other hand, local optimization methods converge fast, thus allowing for exhaustive searches with various initial points. Such searches are not feasible with global optimization methods, which are slower and more difficult to steer through an initial guess and converge to a realizable solution. Nonetheless, there exists an opportunity for further investigation to rigorously define the underlying SRFT model features leading to unrealizable solutions, thereby providing guidelines for the selection of the initial guess as well as the formulation of constraints to steer the optimization away from such solutions. Finally, we have demonstrated that the improved SRFT ensures realizable IMN solutions. The systematic approach in this paper enables us to find a UWB IMN solution with an 81.3% power reduction and an amplifier f_T at around 100 GHz to ensure the amplifier operates at 10.6 GHz.

Author Contributions: Conceptualization, S.H. and C.-H.C.; methodology, S.H. and C.-H.C.; software, S.H.; validation, S.H., C.-H.C. and N.K.N.; formal analysis, S.H.; investigation, S.H. and C.-H.C.; writing—original draft preparation, S.H.; writing—review and editing, S.H., C.-H.C. and N.K.N.; visualization, S.H. and C.-H.C.; supervision, C.-H.C. and N.K.N.; funding acquisition, C.-H.C. and N.K.N. All authors have read and agreed to the published version of the manuscript.

Funding: This research was funded by Natural Sciences and Engineering Research Council: RTI-2020-00456, RGPIN-2017-06058, RGPIN-2020-05706.

Data Availability Statement: Data is contained within the article.

Conflicts of Interest: The authors declare no conflict of interest.

References

1. Fontana, R.J. Recent system applications of short-pulse ultra-wideband (UWB) technology. *IEEE Trans. Microw. Theory Tech.* **2004**, *52*, 2087–2104. [CrossRef]
2. Yarman, B.S. Real frequency techniques a historical review. In *Design of Ultra Wideband Antenna Matching Networks*; Yarman, B.S., Ed.; Springer Science + Business Media B. V.: Dordrecht, The Netherlands, 2008; pp. 1–8.
3. Fano, F.M. Theoretical limitations on the broadband matching of arbitrary impedances. *J. Frankl. Inst.* **1950**, *249*, 57–83. [CrossRef]
4. Youla, D.C. A new theory of broadband matching. *IEEE Trans. Circuit Theory* **1964**, *11*, 30–50. [CrossRef]
5. Carlin, H.J. A new approach to gain-bandwidth problems. *IEEE Trans. Circuits Syst.* **1977**, *24*, 170–175. [CrossRef]
6. Carlin, H.J.; Amstutz, P. On optimum broadband matching. *IEEE Trans. Circuits Syst.* **1981**, *28*, 401–405. [CrossRef]
7. Breed, G. *Improving the Bandwidth of Simple Matching Networks*; Summit Technical Media, LLC: Bedford, NH, USA, 2008; pp. 56–60.
8. Yang, H.; Kim, K. Ultra-wideband impedance matching technique for resistively loaded vee dipole antenna. *IEEE Trans. Antennas Propagat.* **2013**, *66*, 5788–5792. [CrossRef]
9. Bevilacqua, A.; Niknejad, A.M. An ultrawideband CMOS low-noise amplifier for 3.1–10.6-GHz wireless receivers. *IEEE J. Solid-State Circuits* **2004**, *39*, 2259–2268. [CrossRef]
10. Ismail, A.; Abidi, A.A. A 3–10-GHz low-noise amplifier with wideband LC-ladder matching network. *IEEE J. Solid-State Circuits* **2004**, *39*, 2269–2277. [CrossRef]
11. Zhao, C.; Duan, D.; Xiong, Y.; Liu, H.; Yu, Y.; Wu, Y.; Kang, K. A K-/Ka-band broadband low-noise amplifier based on the multiple resonant frequency technique. *IEEE Trans. Circuits Syst. I* **2022**, *69*, 3202–3211. [CrossRef]
12. Zailer, E.; Belostotski, L.; Plume, R. Wideband LNA noise matching. *IEEE J. Solid-State Circuits Lett.* **2020**, *3*, 62–65. [CrossRef]
13. Carlin, H.J.; Yarman, B.S. The double matching problem: Analytic and real frequency solutions. *IEEE Trans. Circuits Syst.* **1983**, *30*, 15–28. [CrossRef]
14. Fettweis, A. Parametric representation of Brune functions. *Int. J. Circuit Theory Appl.* **1979**, *7*, 113–119. [CrossRef]
15. Yarman, B.S.; Carlin, H.J. A simplified "real frequency" technique applied to broad-band multistage microwave amplifiers. *IEEE Trans. Microw. Theory Tech.* **1982**, *30*, 2216–2222. [CrossRef]
16. Carlin, H.J.; Civalleri, P. On flat gain with frequency-dependent terminations. *IEEE Trans. Circuits Syst.* **1985**, *32*, 827–839. [CrossRef]
17. Jarry, P.; Beneat, J.N. *Microwave Amplifier and Active Circuit Design Using the Real Frequency Technique*; John Wiley & Sons, Inc.: Hoboken, NJ, USA, 2016.
18. Wu, D.Y.-T.; Mkadem, F.; Boumaiza, S. Design of a Broadband and Highly Efficient 45W GaN Power Amplifier via Simplified Real Frequency Technique. In Proceedings of the IEEE MTT-S International Microwave Symposium, Anaheim, CA, USA, 23–28 May 2010.
19. Carlin, H.J. The scattering matrix in network theory. *IRE Trans. Circuit Theory* **1956**, *3*, 88–97. [CrossRef]
20. Limand, J.S.; Park, D.C. A modified Chebyshev bandpass filter with attenuation poles in the stopband. *IEEE Trans. Microw. Theory Tech.* **1997**, *45*, 898–904.
21. Yeung, L.K.; Wu, K.-L. A compact second-order LTCC bandpass filter with two finite transmission zeros. *IEEE Trans. Microw. Theory Tech.* **2003**, *51*, 337–341. [CrossRef]
22. Yarman, B.S.; Fettweis, A. Computer-aided double matching via parametric representation of Brune functions. *IEEE Trans. CAS* **1990**, *37*, 212–222. [CrossRef]
23. Bode, H.W. *Network Analysis and Feedback Amplifier Design*; D. Van Nostrand Co., Ltd.: New York, NY, USA, 1945; pp. 350–371.
24. Steer, M. *Microwave and RF Design Networks*, 3rd ed.; NC State University: Raleigh, NC, USA, 2019.
25. Matthaei, G.; Young, L.; Jones, E.M.T. *Microwaves Filters, Impedance-Matching Networks, and Coupling Structures*; McGraw-Hill: New York, NY, USA, 1985.

26. Dai, Z.; He, S.; You, F.; Peng, J.; Chen, P.; Dong, L. A new distributed parameter broadband matching method for power amplifier via real frequency technique. *IEEE Trans. Microw. Theory Tech.* **2015**, *63*, 449–458. [CrossRef]
27. Lera, G.; Pinzolas, M. Neighborhood based Levenberg–Marquardt algorithm for neural network training. *IEEE Trans. Neural Netw.* **2002**, *13*, 1200–1203. [CrossRef]
28. Sengül, M. Design of practical broadband matching networks with lumped elements. *IEEE Trans. Circuits Syst. II* **2013**, *60*, 552–556. [CrossRef]
29. Temes, G.C.; Lapatra, J.W. *Introduction to Circuit Synthesis and Design*; McGraw-Hill: New York, NY, USA, 1977.
30. Köprü, R. FSRFT—Fast simplified real frequency technique via selective target data approach for broadband double matching. *IEEE Trans. Circuits Syst. II Express Briefs* **2017**, *64*, 141–145.
31. Yegin, K.; Martin, A.Q. On the design of broadband loaded wire antennas using the simplified real frequency technique and a genetic algorithm. *IEEE Trans. Antennas Propagat.* **2003**, *51*, 220–228. [CrossRef]
32. Gerkis, A.N. Broadband impedance matching using the real frequency network synthesis technique. *Appl. Microw. Wirel.* **1998**, *10*, 26–36.
33. Bellomo, A.F. Gain and noise considerations in RF feedback amplifier. *IEEE J. Solid-State Circuits* **1968**, *3*, 290–294. [CrossRef]
34. Meyer, R.G.; Mack, W.D. A 1-GHz BiCMOS RF front-end IC. *IEEE J. Solid-State Circuits* **1994**, *29*, 350–355. [CrossRef]
35. Shaeffer, D.K.; Lee, T.H. A 1.5-V, 1.5-GHz CMOS low noise amplifier. *IEEE J. Solid-State Circuits* **1997**, *32*, 745–759. [CrossRef]